Petroleum Science 23 (2026) 3602–3615

Contents lists available at ScienceDirect

Petroleum Science

journal homepage: www.keaipublishing.com/en/journals/petroleum-science

Original Paper

Residual magnetic fields from magnetic flux leaking detection accelerate microbiologically influenced corrosion of X80 pipeline steel induced by *Desulfovibrio desulfuricans* in sea mud environment

Ya-Jun Gai, Jia-Hang Li *, Fei Xie **, Dan Wang, Dong-Xu Sun, Yu-Xin Wang, Ming Wu

Key Laboratory of Oil and Gas Storage and Transportation Technology, College of Petroleum Engineering, Liaoning Petrochemical University, Fushun 113001, Liaoning, China

ARTICLE INFO

Article history:
Received 1 April 2025
Received in revised form
20 September 2025
Accepted 16 January 2026
Available online 21 January 2026

Edited by Teng Zhu and Meng-Jiao Zhou

Keywords:
Pipeline
Magnetic flux leakage
Magnetic field
Sulfate-reducing bacteria
Microbially influenced corrosion
Sea mud

ABSTRACT

Subsea pipelines buried in marine sediments are highly susceptible to microbiologically influenced corrosion (MIC). Although magnetic flux leakage (MFL) inspection is widely employed for pipeline integrity assessment, the effect of residual magnetic fields (MF) on MIC remains poorly understood. In this study, the effect of MFs on the MIC behavior of X80 pipeline steel induced by *Desulfovibrio desulfuricans* was systematically investigated. The results show that MF slightly accelerate the abiotic corrosion of X80 steel, while MF enhances mass transfer at the metal–electrolyte interface via Lorentz force. While MFs have little influence on the growth of *D. desulfuricans* utilizing organic carbon sources, they significantly promote extracellular electron transfer by activating magnetite (Fe_3O_4). This enhancement enables *D. desulfuricans* to more efficiently acquire electrons from the metal surface. These findings provide critical guidance for MFL inspection practices in offshore oil and gas pipelines, suggesting that residual MF will accelerate MIC. Therefore, the potential risk of MIC should be carefully considered when applying magnetic inspection technologies in microbially active environments.

1. Introduction

The growing global demand for energy has intensified the depletion of terrestrial oil and gas resources, thereby accelerating the exploration and development of marine hydrocarbon reserves as a viable alternative. The South China Sea, endowed with abundant petroleum and natural gas deposits, exhibits remarkable potential for offshore energy exploitation. Pipeline systems constitute the primary means for oil and gas transportation. However, the complex marine environment harbors diverse microbial communities, among which microbiologically influenced corrosion (MIC) poses a major threat to pipeline integrity (Wang et al., 2024a; Li et al., 2025a). The maintenance costs and technical challenges associated with repairing offshore pipelines far exceed those of onshore systems, underscoring the need for enhanced strategies to ensure pipeline safety and durability. Statistical analyses indicate that MIC accounts for approximately 20% of total corrosion-related losses in marine environments (Hashemi et al., 2017). As facultative anaerobes, sulfate-reducing bacteria (SRB) utilize sulfate as terminal electron acceptors during anaerobic respiration and exhibit widespread distribution in both marine and terrestrial environments (Liu et al., 2022a; Javed et al., 2024). SRB have been identified as the primary causative agent of microbial corrosion in marine oil and gas infrastructure (Zhang et al., 2024a; Li et al., 2025b). Therefore, elucidating the corrosion mechanisms induced by SRB on pipeline steels in marine environments is crucial for safeguarding the operational reliability and structural integrity of offshore pipeline systems.

The participation of microorganisms in metal corrosion was first reported as early as 1910 (Gaines, 1910). The cathodic depolarization theory, initially proposed to explain MIC induced by SRB, suggested that SRB enhance corrosion by consuming cathodic hydrogen (Kuhr and Van, 1934; Spruit and Wanklyn, 1951; Wanklyn and Spruit, 1952). Dinh et al. (2004) found a novel SRB strain, *Desulfovibrio ferrophilus* IS5, capable of directly extracting electrons from metallic surfaces to sustain its metabolic activity. This finding fundamentally advanced

* Corresponding author.
** Corresponding author.
E-mail addresses: ljh970404@163.com (J.-H. Li), xiefei0413@163.com (F. Xie).
Peer review under the responsibility of China University of Petroleum (Beijing).

https://doi.org/10.1016/j.petsci.2026.01.023

the understanding of MIC mechanisms, revealing that certain SRB species can bypass traditional hydrogen-mediated pathways and engage in direct electron uptake from metals. Then biocatalytic cathodic sulfate reduction (BCSR) theory colleagues thermodynamically confirms the feasibility of SRB uptaking electrons from metals (Fe^0) (Xu and Gu, 2014). Currently, SRB induced MIC is primarily categorized into two mechanisms. The first involves the acquisition of electrons from metals via extracellular electron transfer (EET). Recently, EET-MIC has been demonstrated in the MIC of a variety of electroactive microorganisms (Lu et al., 2024, 2025). The second mechanism involves metabolite-induced MIC (M-MIC), arises from the production of corrosive metabolites, such as H_2S (Cristiani et al., 2025; Lekbach et al., 2021).

To detect corrosion in subsea pipelines and ensure their safe operation, magnetic flux leakage (MFL) detection technology has been extensively employed to evaluate marine pipeline integrity. However, residual magnetic fields (MF) remaining after MFL inspection will reduced the corrosion resistance of pipeline (He et al., 2023; Wang et al., 2023). The Lorentz forces and magnetic gradient forces generated by residual MF can facilitate ion migration, thereby accelerating pipeline steel corrosion (Zhao et al., 2021; Wang et al., 2022a). Beyond abiotic corrosion, the effect of MF on MIC warrants significant attention. MF have been reported to enhance the EET capability of *Shewanella putrefaciens* (Wang et al., 2024b). Additionally, magnetic fields can activate magnetic nanoparticles to accelerate MIC induced by *Desulfovibrio* species (Wang et al., 2022b; Alrammah et al., 2024). Magnetite can also compensate for the absence of pilin-associated *c*-type cytochromes in microbial electron transport chains, thereby improving EET efficiency (Liu et al., 2015; Jin et al., 2023).

While some research indicates that MF exhibit bactericidal effects through microbial growth inhibition, this phenomenon is not universally applicable across all microorganisms (Li et al., 2024; Lin et al., 2024). Liu et al. (2016) revealed that MF could suppress the growth of iron-oxidizing bacteria and consequently mitigate MIC. Zheng et al. (2013) also demonstrated MF inhibited the MIC induced by SRB on 304 stainless steels. Conversely, Liu et al. (2018) observed that MF could alter the spatial arrangement of extracellular polymeric substances secreted by microorganisms, facilitating ion penetration to material surfaces and accelerating corrosion. These conflicting reports highlight the ambiguity surrounding the mechanisms of MF effects on MIC.

To address this knowledge gap, priority should be given to elucidating the impact of MF on MIC induced by SRB. Considering that MIC is closely associated with EET and acid production through metabolic activities, a systematic investigation into MF effects on these two critical pathways is imperative. We firstly evaluated the effect of MF on SRB growth and metabolic activity through comparative analysis of cellular proliferation dynamics and sulfate reduction capacity. Then the corrosion behavior was analyzed through integrated methodologies including weight loss quantification, pitting corrosion assessment, corrosion product characterization, and electrochemical measurements. Finally, the effect of MF on M-MIC was elucidated by monitoring pH fluctuations, while the effect of MF on EET-MIC mechanisms was investigated through cyclic voltammetry (CV) measurements. The elucidation of MF effects on MIC mechanisms in marine environments holds crucial implications for developing corrosion mitigation strategies in submarine pipelines.

2. Experimental procedures

2.1. Materials and bacterial cultivation

API 5L X80 pipeline steel with the chemical composition of (w/w) C 0.049%, Si 0.18%, Mn 1.82%, P 0.012%, S 0.0002%, Mo 0.08%, Ni 0.24%, V 0.0001%, Cr 0.026%, N 0.01%, Cu 0.14% and balance Fe were used in this work. The coupons (10 mm × 10 mm × 3 mm) were abraded to 1200-grit, degreased with acetone, dehydrated in anhydrous ethanol, and preserved in a drying cabinet. To simulate the post-MFL residual MF environment, a $Nd_2Fe_{14}B$ (neodymium-iron-boron) permanent magnet was affixed to the coupon's reverse side, generating a surface magnetic flux density of 20 mT as verified by a calibrated gaussmeter.

Sea mud was collected from the South China Sea and analyzed by Fourier Transform Infrared Spectrometer (FT-IR, Nicolet Is 50, Thermo Fisher Scientific, USA), high-resolution nuclear magnetic resonance spectroscopy (HNMR, Avance NEO 600, Bruker, Germany), Gas Chromatography-Ion Mobility Spectrometry (GC-IMS, FlavourSpec1H1-00053, G.A.S., Germany) and X-ray fluorescence spectrometry (XRF, PANalytical Axios, PANalytical B.V., Netherlands) for physical and chemical properties (Supporting Material). It was determined that the sea mud contained 13.89 g of Na_2SO_4, 27.78 g of KCl and 16.44 g of $MgSO_4$. The pH value of the sea mud was 7.8.

The SRB strain (*Desulfovibrio desulfuricans*) used in this study was isolated from marine mud in the South China Sea, and the exact isolation procedure can be found in our previous work (Sun et al., 2018). Enriched simulated seawater medium with 1 g/L yeast extract and 3.5 g DL-sodium lactate as an electron donor was used in this work. The medium was filtered and sterilized, then nitrogen (99.9%) was passed into the medium for 1 h, and the pH of medium was adjusted to 7.8 ± 0.2 used 10% HCl (v/v) and 10% NaOH (w/w). Then the medium was sterilized at 121 °C for 15 min. Based on the actual content of SRB in the marine mud, 1% SRB seeds were inoculated into the medium. All operations were performed in a sterile nitrogen-filled glove box. The SRB culture was incubated at 30 °C. During microbial cultivation, paired $Nd_2Fe_{14}B$ magnets were symmetrically positioned along opposing sides of polycarbonate culture tubes to establish a uniform MF. The MF intensity was precisely maintained at 20 mT through iterative adjustments of magnet dimensions and spatial separation.

2.2. Sulfate consumption and hydrogen sulfide production

Planktonic cell quantification was performed using a hemocytometer under 400× magnification optical microscopy. For sessile cell enumeration, biofilm-associated cells were carefully detached from substrate surfaces using a sterile cell scraper, subsequently resuspended in sterile phosphate-buffered saline (PBS), and quantified through hemocytometric analysis. The sulfate concentration was analyzed using ion chromatography instrument (IC, DIONEXICS-1100, Thermofisher Scientific, USA). To assess the effect of MF on the EET behavior of *Desulfovibrio desulfuricans* (*D. desulfuricans*), the sodium lactate in the EASW medium was removed, and X80 coupons were used as the sole electron donor for a 14-day co-culture with the cells. The sulfate concentration in the medium were monitored during the cultivation cycle.

2.3. Biofilm and surface morphology analysis

The biofilm on the coupons surface were characterized after incubated for 7 d and 14 d. The coupons were washed in sterile PBS solution, and the biofilm was fixed with 2.5% (v/v) glutaraldehyde for 8 h, then dehydrated with serial dilutions of ethanol (50%, 60%, 70%, 80%, 90% and 100%) for 5 min before observation. The biofilm was sputtered with gold powder to ensure conductivity and observed using field emission scanning electron microscope (FESEM, SU8010, HITACHI, Japan). The live and dead bacterial cells were stained using the mixed SYTO-9 dye and propidium iodide dye for 10 min and characterized using confocal laser scanning

microscope (CLSM, C2 Plus, Nikon, Japan). The chemical composition of the biofilm was characterized using energy-dispersive X-ray spectroscopy (EDS, XFlash Detector 5030, Bruker, Germany). After immersed for 14 d, the corrosion products were analyzed using X-ray photoelectron spectroscopy (XPS, ESCALAB 250Xi+, Thermo Fisher Scientific, MA, USA).

2.4. Corrosion tests

The coupons were ultrasonically cleaned with a descaling solution (50 mL of concentrated hydrochloric acid, 50 mL of deionized water and 1 g of hexamethylenetetramine) after immersed for 14 d. The corrosion morphology of the coupons' surface was observed using CLSM. The weight loss was calculated by measuring the mass of the coupons before and after immersion using an analytical balance (ME204E, Mettler Toledo, Switzerland), with a minimum of five replicate experiments prepared for each test.

2.5. Electrochemical tests

The electrochemical tests were performed on an electrochemical workstation (PARSTAT 2273, Princeton, USA). The three-electrode system was constructed with X80 steel as the working electrode (WE), platinum sheet as the counter electrode (CE), and saturated calomel electrode (SCE) as the reference electrode (RE). After the open circuit potential has stabilized, linear polarization resistance (LPR) and electrochemical impedance spectroscopy (EIS) tests were conducted. The LPR scan was performed within a range of −10 mV to 10 mV (vs. OCP) at a scan rate of 0.1667 mV/s. The EIS test was carried out over a frequency range from 10^5 Hz to 10^{-2} Hz with an applied perturbation amplitude of 10 mV. Following the completion of the 14-d testing period, a potentiodynamic polarization test was conducted, scanning from −0.3 V to 0.3 V (vs. OCP) at a scan rate of 0.1667 mV/s. In the cyclic voltammetry (CV) tests, graphite was employed as the working electrode. The potential range was set from −1.0 V to 0.1 V vs. SCE, and the scan rates were configured at 10 mV/s.

3. Results

3.1. Cell counts, biofilm characterization and broth's pH

Fig. 1(a)–(d) show the biofilm formation on coupons cultured for 7 d and 14 d under control and MF environment. Distinct curved cell structures can be clearly identified among the sessile cells, consistent with the characteristic morphology of the *Desulfovibrio* genus. EDS analysis indicates that the biofilm primarily consists of iron, sulfur, oxygen, and nitrogen elements (Fig. 1(e)–(h)). Among these, iron, oxygen, and sulfur are derived from corrosion products, while nitrogen is the primary component of proteins in the biofilm. The normalized concentrations of these four elements exhibit close similarity across varying experimental conditions.

The cell viability was assessed by live-dead staining. CLSM images showed the ratio of live/dead cells in the biofilm is close (Fig. 2(a) and (b)). The effect of MF on the biofilm-forming capacity was evaluated using crystal violet staining. As crystal violet binds specifically to biofilm components, the absorbance of the solution quantitatively reflects the amount of adherent biofilm biomass (Li et al., 2021). As shown in Fig. 2(c), MF has little effect on cell count. After 14 d of culture under control conditions, the counts of planktonic and adherent cells were $(2.5 \pm 0.6) \times 10^7$ and $(8.2 \pm 2.1) \times 10^7$, respectively (Fig. 2(d)). The number of planktonic cells exceeded that of sessile cells, which can be attributed to planktonic cells having easier access to organic nutrients. In contrast, sessile cells in the biofilm are potentially subject to diffusion limitations of organic nutrients. Under MF condition, both planktonic and sessile cell counts decreased slightly to $(1.4 \pm 0.4) \times 10^7$ and $(4.4 \pm 1.5) \times 10^7$, respectively. Sulfate reduction capacity is a critical indicator of SRB metabolic activity. Under MF condition, the sulfate reduction capacity of cells is comparable to that in control condition (Fig. 2(e)), which is align with the cell count results. The pH value of SRB broth decreased from 7.8 to 7.0 following 14 days of culture (Fig. 2(f)). The acidification of culture medium is associated with H_2S production during bacterial metabolism. However, the limited acidification of the medium can be explained by FeS precipitation and the restricted solubility of H_2S, which collectively buffer significant pH reduction (Jia et al., 2018). The neutral environment also precludes M-MIC (Zhang et al., 2024b).

3.2. Corrosion test

Fig. 3(a)–(d) present the surface morphologies of the coupons after removal of corrosion products and the corresponding cross-sectional profiles. The coupons in the abiotic medium exhibited a maximum pit depth of 5.2 μm (Fig. 3(a)). Under MF condition, the maximum pit depth increased to 6.2 μm (Fig. 3(b)), indicating that the MF significantly enhanced the pitting corrosion of X80 steel. The maximum pitting depth of coupon in SRB broth reached 24.3 μm, highlighting the aggressively MIC induced by SRB (Fig. 3(c)). Under MF condition, the maximum pitting depth of coupon in SRB broth reached 33.5 μm (Fig. 3(d)).

The pit density was statistically analyzed: control (205 ± 54 pits/cm^2), MF (463 ± 51 pits/cm^2), SRB (1380 ± 220 pits/cm^2), and SRB + MF (2200 ± 210 pits/cm^2) (Fig. 4(a)). Both the average and maximum pit depths, along with pit diameter measurements, consistently revealed the same corrosion severity hierarchy: SRB + MF > SRB > MF > control (Fig. 4(b)). Although MF markedly accelerated pitting corrosion, its effect on uniform corrosion was negligible. The weight loss differences between the control (0.6 ± 0.1 mg) group and the MF group (0.7 ± 0.1 mg) were small (Fig. 4(c)). In contrast, the weight loss of coupons in SRB broth was 11.2 ± 0.5 mg, further exacerbated to 13.8 ± 0.4 mg under the combine effect of SRB and MF (Fig. 4(d)). The above results confirm the synergistic interaction between MF and microbiological activity, demonstrating that MF preferentially enhances MIC rather than abiotic corrosion.

3.3. Analysis of corrosion product

Fig. 5(a)–(d) show the high-resolution XPS spectra of Fe 2p3/2 and S 2p3/2 for corrosion products formed on X80 steel coupons after 14-d immersion. The Fe 2p3/2 spectra showed characteristic peaks at 710.4, 711.4, and 711.8 eV, corresponding to Fe^0, Fe^{2+} species (Fe_3O_4, FeO and FeOOH), and Fe^{3+} species (Fe_2O_3 and Fe_3O_4), respectively. Quantitative analysis through spectral fitting revealed significant variations in the relative proportions of these iron oxidation states across different environments. The coupons immersed in SRB broth demonstrated a reduction in Fe^0 content, which is attributed to the biofilm coating.

The S 2p3/2 spectra displayed distinct environmental dependencies. No discernible sulfur-related signals were detected on coupons exposed to sterile conditions after 14-d of immersion. While characteristic sulfur peaks can be found in SRB broth, which are correspond to iron sulfide compounds (FeS and FeS_2). The presence of iron sulfides provides direct spectroscopic evidence of MIC induced by SRB (Ma et al., 2024; Zhang et al., 2024b). The comparative spectral data conclusively demonstrate that SRB activity significantly alters corrosion products through biogenic sulfide generation, distinguishing MIC from abiotic corrosion.

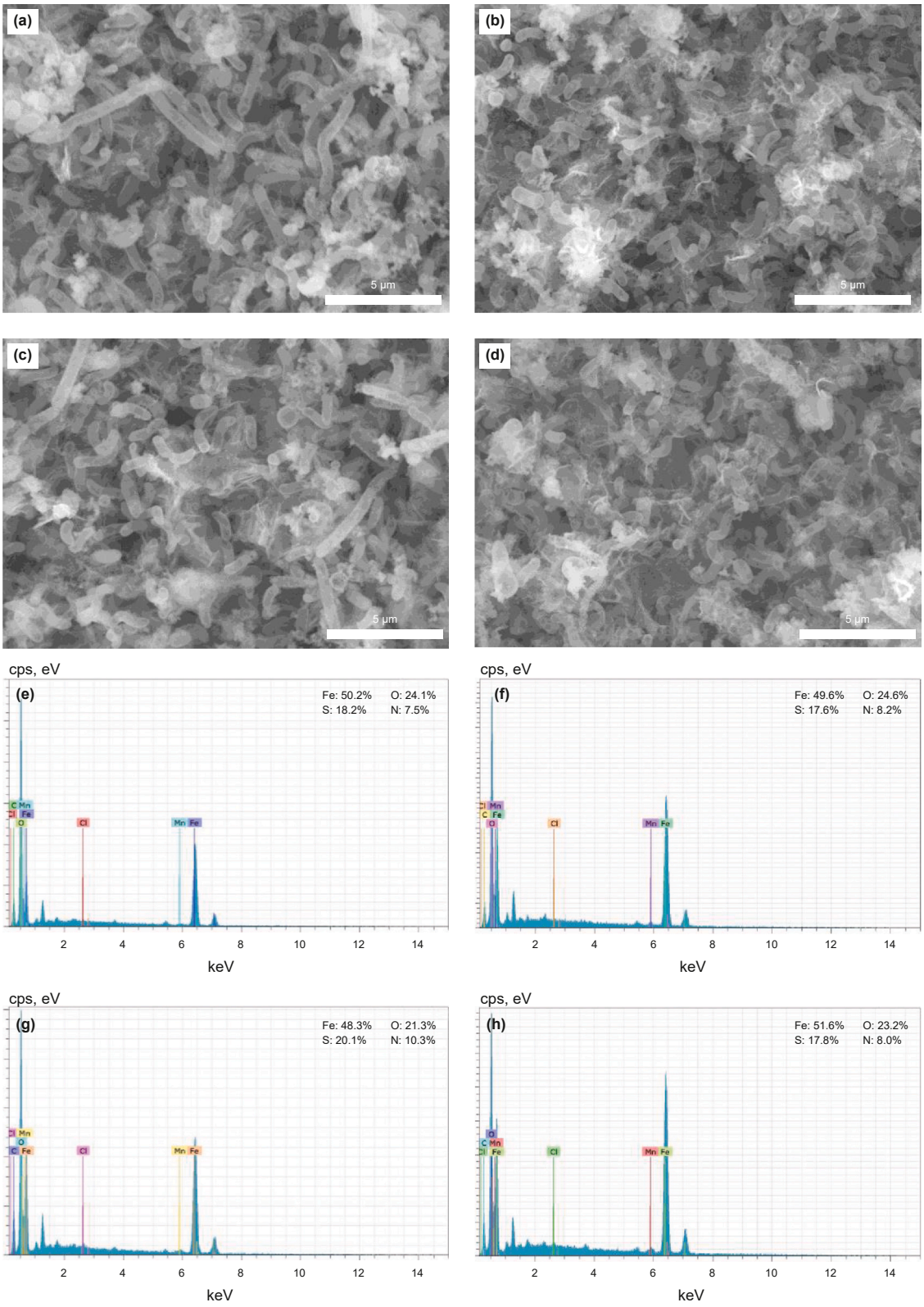

Fig. 1. **(a)**–**(d)** SEM images and **(e)**–**(h)** corresponding EDS spectra of biofilms formed under different conditions: **(a)–(e)** 7 d of immersion without MF, **(b)–(f)** 14 d of immersion without MF, **(c)–(g)** 7 d of immersion with MF, and **(d)–(h)** 14 d of immersion with MF.

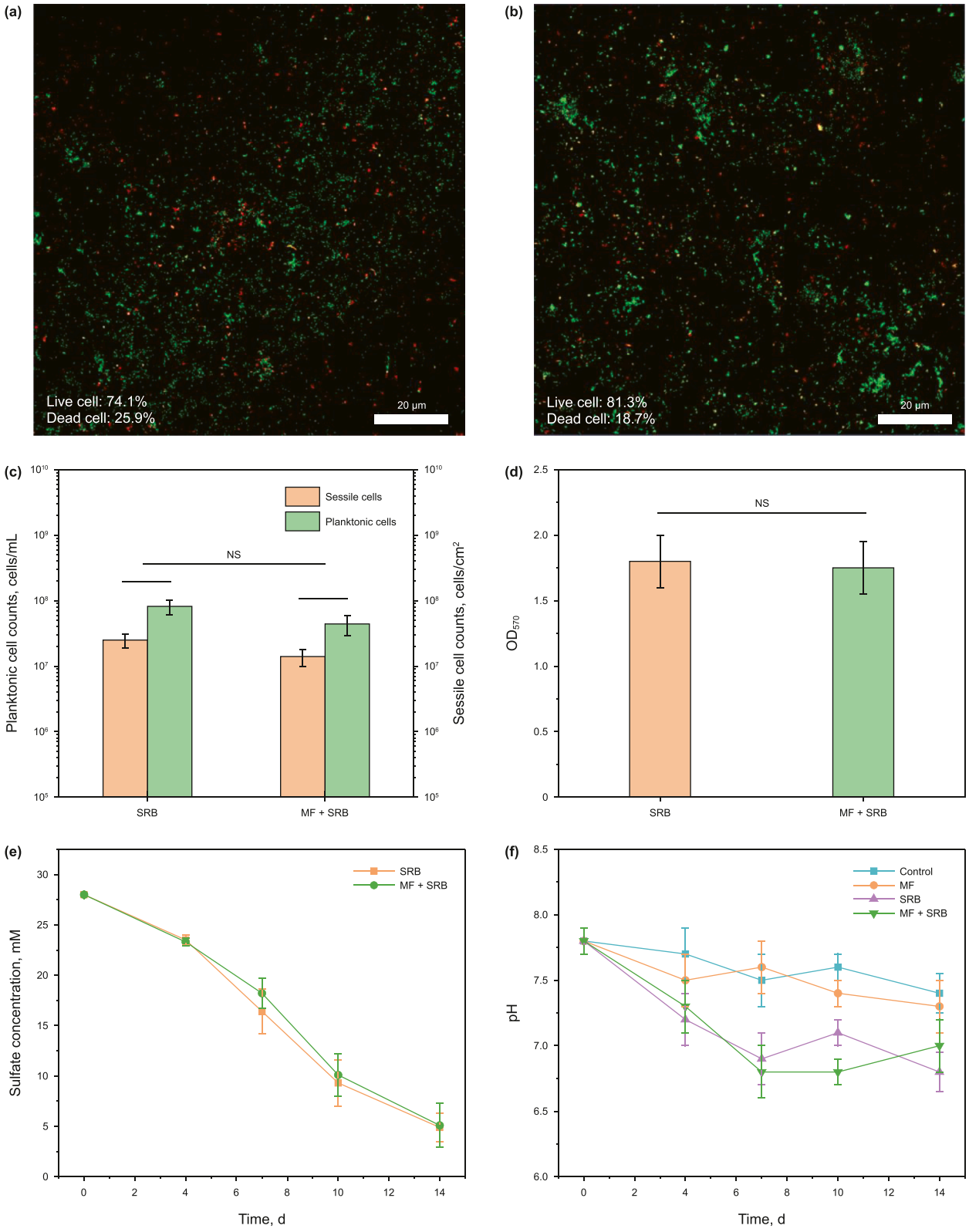

Fig. 2. (**a**) CLSM images of biofilms formed under control condition, (**b**) CLSM images of biofilms formed under MF condition, (**c**) planktonic and sessile cell counts after 14 d incubation, (**d**) OD_{570}, (**e**) variations in sulfate concentration of SRB broth during 14 d of incubation, and (**f**) variations in the pH values of medium during 14 d of incubation.

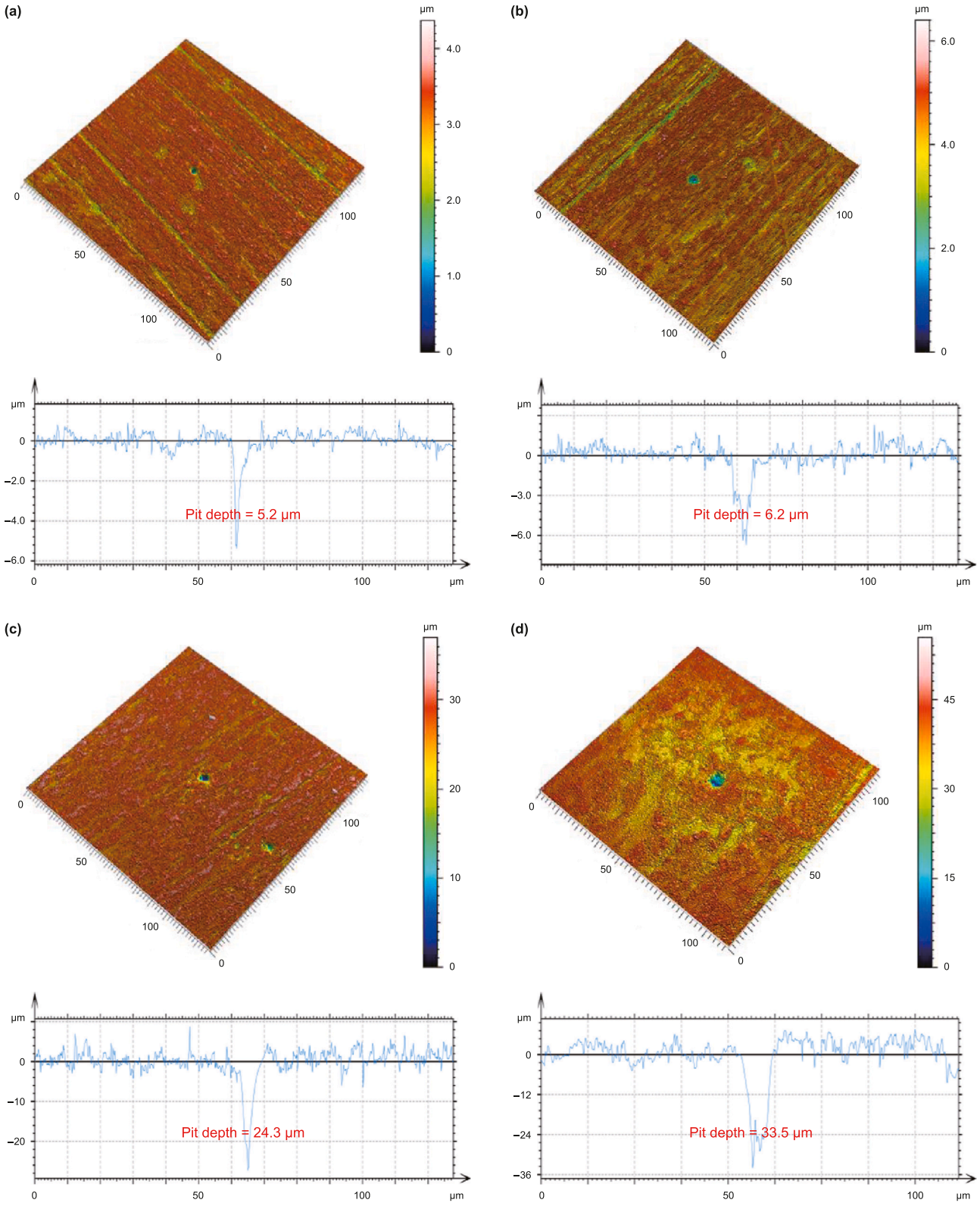

Fig. 3. 3D-CLSM images and corresponding depth profiles of the deepest pits formed on X80 steel coupons after 14 d of immersion under different conditions: **(a)** in sterile medium without MF, **(b)** in sterile medium with MF, **(c)** in SRB broth without MF, and **(d)** in SRB broth with MF.

3.4. Electrochemical measurements

Fig. 6(a) shows the E_{OCP} values of X80 steel coupons. In the abiotic medium, the E_{OCP} value stabilized at −677 ± 5 mV under control conditions. Under MF condition, the E_{OCP} value negative shifted about 20 mV, maintaining at −698 ± 5 mV. In the SRB broth, the E_{OCP} value stabilized at −754 ± 6 mV, with MF exhibiting negligible effects on E_{OCP}. The negative E_{OCP} values indicate enhanced thermodynamic

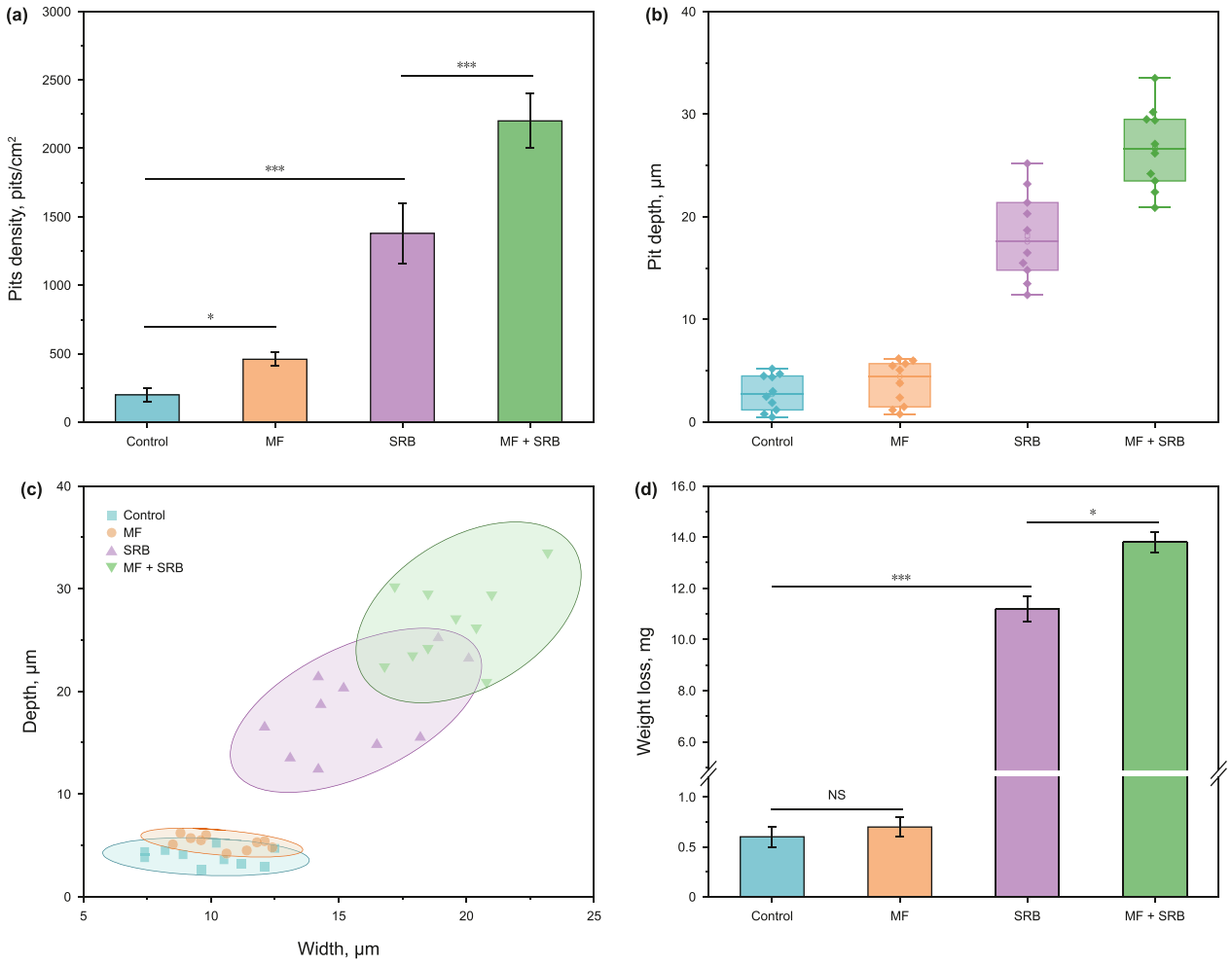

Fig. 4. Pit analysis and weight loss: **(a)** pit density, **(b)** the box chart of pit depth (the box chart is composed of five lines, from top to bottom, which are the maximum value, third quartile, median, quarter quantile and minimum value of the coupon index. The dots are the mean value), **(c)** distributions of pit depth and width, and **(d)** weight loss.

susceptibility to corrosion. As shown in Fig. 6(b), the polarization resistance (R_p) of X80 steel in abiotic medium was 3005 ± 132 Ω·cm^2 under non-magnetic conditions, decreasing by 10%–2711 ± 154 Ω·cm^2 upon MF application. In SRB broth, the R_p values were markedly lower, registering 312 ± 32 Ω·cm^2 (SRB) and 279 ± 28 Ω·cm^2 (MF + SRB), respectively. The lower R_p values correlate with higher corrosion rate (Li et al., 2026). The potentiodynamic polarization curves (Fig. 6(c)) and corresponding Tafel-extracted parameters (Fig. 6(d)) revealed the corrosion current density (i_{corr}) and corrosion potential (E_{corr}). In abiotic medium, E_{corr} values were −664 ± 7 mV (control) and −674 ± 5 mV (MF). In SRB broth, the E_{corr} shifts to −793 ± 10 mV (SRB) and −814 ± 6 mV (MF + SRB), respectively, aligning with the E_{OCP} trends. Notably, i_{corr} values increased from 0.6 ± 0.1 μA/cm^2 (control) to 0.8 ± 0.1 μA/cm^2 (MF) in abiotic medium. In SRB broth, i_{corr} values further rising to 12.6 ± 1.1 μA/cm^2 (SRB) and 19.9 ± 1.5 μA/cm^2 (MF + SRB), respectively.

Fig. 7 shows the Nyquist and Bode plots of X80 steel coupons. The capacitive arc diameters observed in SRB broth were significantly smaller than those in abiotic medium, indicating enhanced corrosive activity under biotic conditions. This conclusion is further supported by the reduced impedance modulus in the low-frequency region ($|Z|_{0.01Hz}$) of the Bode plots. Notably, MF further diminished the capacitive arc diameters, suggesting an acceleration of corrosion processes by MF.

The EIS data were quantitatively analyzed using an equivalent circuit model (Fig. S5), where R_s, R_f, and R_{ct} represent solution resistance, film resistance, and charge transfer resistance, respectively. Q_f and Q_{dl} were capacitive of the film and electric double layer, with exponent n quantifying the deviation from ideal capacitance. Specifically, R_f reflects the barrier effect of corrosion product layers (mainly Fe oxides and sulfides) against ion migration and electron conduction, while R_{ct} characterizes the kinetic hindrance for interfacial electron exchange between the steel substrate and the surrounding electrolyte or microorganisms. This distinction is critical for understanding the role of residual MF in MIC. At the 14 d, the R_{ct} values for X80 steel were 2694 ± 184 Ω·cm^2 (control) and 2396 ± 147 Ω·cm^2 (MF) in abiotic medium, whereas in SRB broth, R_{ct} decreased to 209 ± 62 Ω·cm^2 (SRB) and 182 ± 25 Ω·cm^2 (SRB + MF) (Table S2). A decrease in R_{ct} indicates facilitated electron transfer, which in our case is consistent with MF-enhanced EET by *D. desulfuricans*. By separating these two resistances, the model enables us to decouple the MF effects on charge transfer kinetics from its effects on film stability, thereby providing more mechanistic insight into the corrosion process. These results demonstrated that the corrosion resistance of X80 coupons in SRB broth were smaller than those in abiotic medium. In addition, both SRB and MF could accelerate the corrosion of X80 coupons.

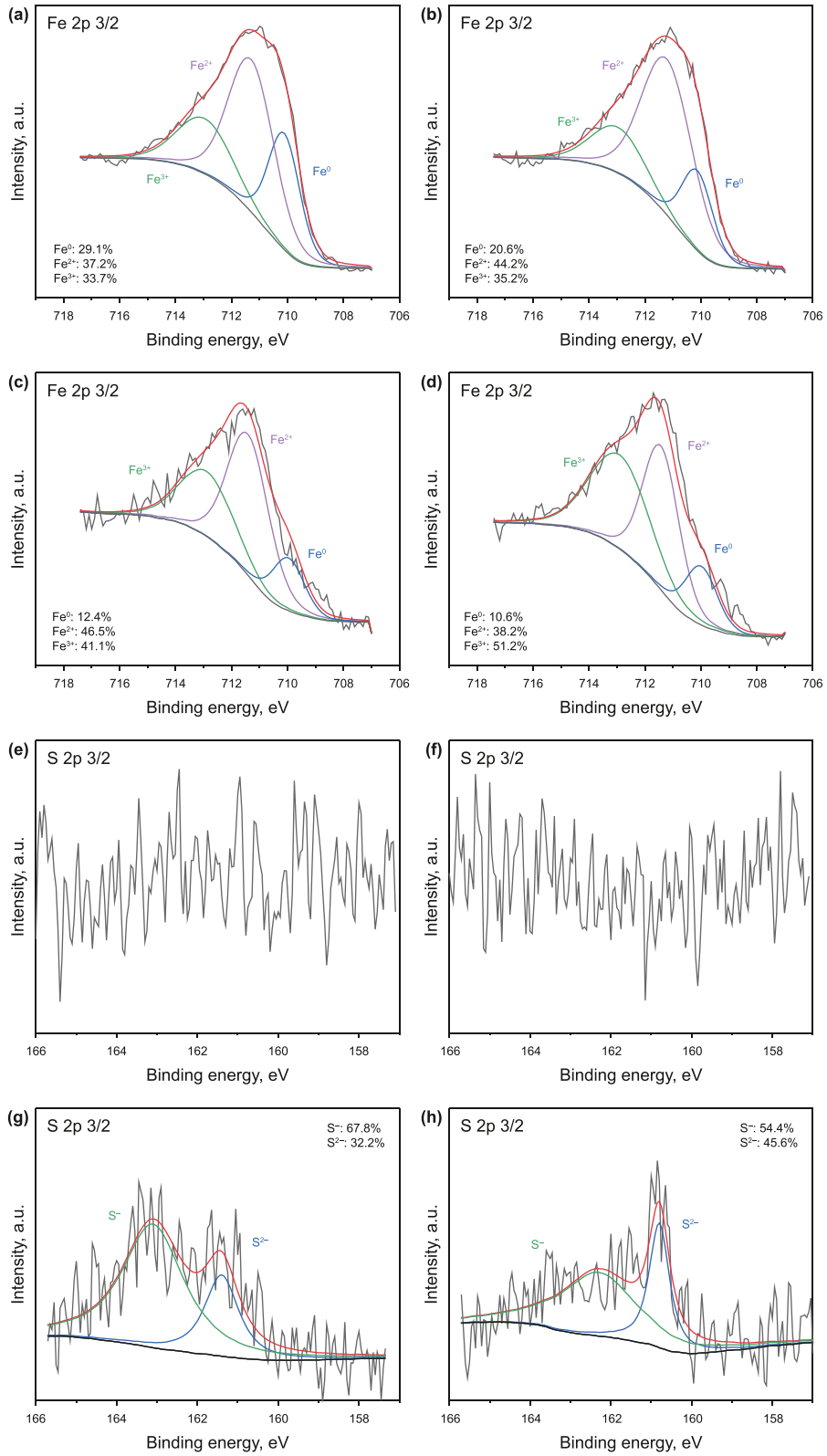

Fig. 5. XPS analysis of corrosion products formed on X80 steel coupons after 14 days of immersion under different conditions: **(a)–(d)** high-resolution Fe 2p 3/2 spectra and **(e)–(h)** high-resolution S 2p 3/2 spectra for **(a)–(e)** abiotic medium without MF, **(b)–(f)** abiotic medium with MF, **(c)–(g)** SRB broth without MF, and **(d)–(h)** SRB broth with MF.

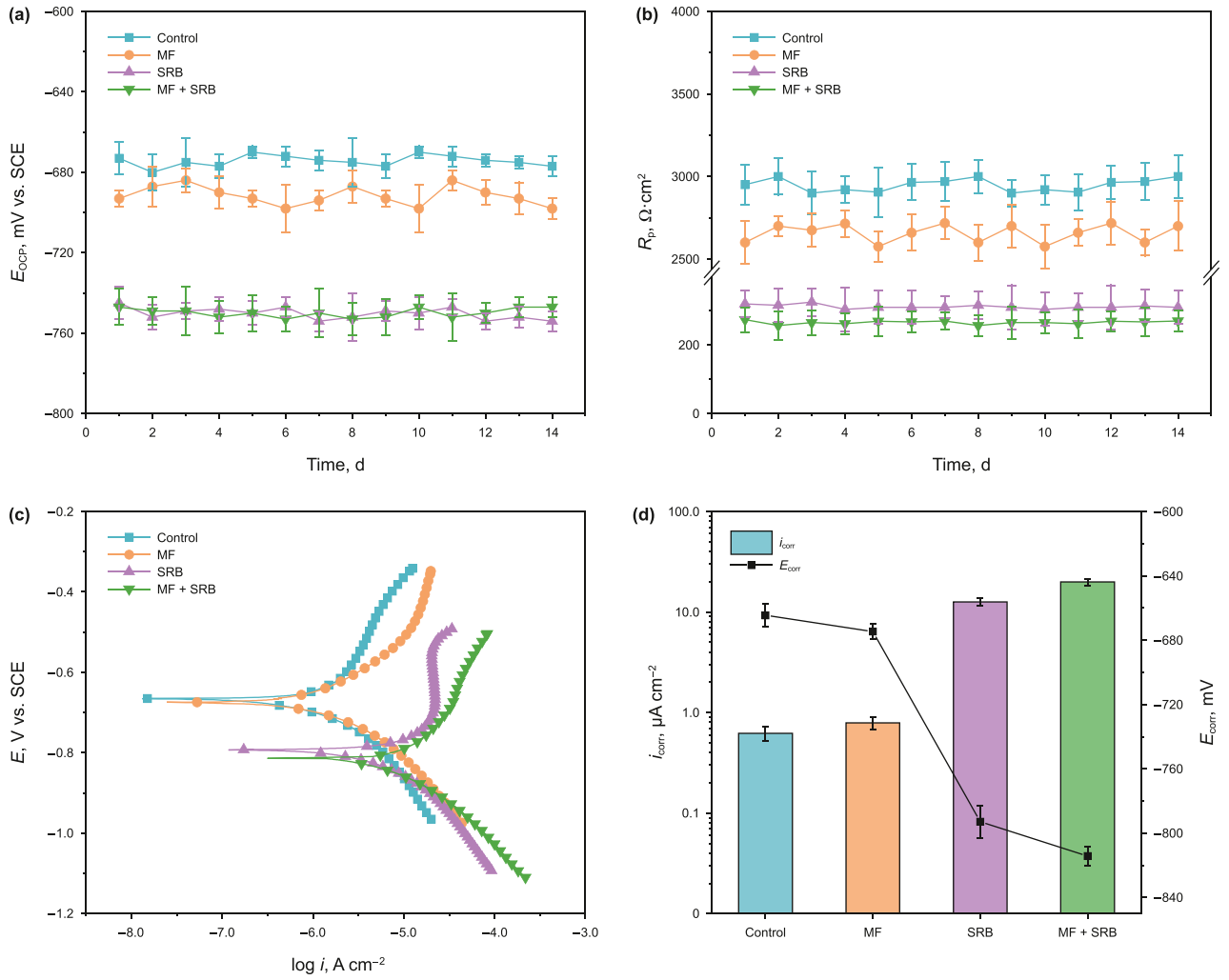

Fig. 6. Eletctrochemical test of X80 coupons: **(a)** E_{OCP}, **(b)** R_p, **(c)** potentiodynamic polarization curves, **(d)** E_{corr} and i_{corr} calculated from **(c)**.

The steady-state CV results under different conditions are shown in Fig. 8(a). No discernible cathodic reduction or anodic oxidation peaks were observed in the abiotic medium, confirming the absence of interfering redox-active components in the culture medium. In contrast, both characteristic cathodic (−0.52 V vs. SCE) and anodic (−0.32 V vs. SCE) peaks were detected in the SRB broth containing *D. desulfuricans*. CV analysis revealed that neither the addition of Fe_3O_4 powder alone nor the sole application of a MF could significantly alter the bioelectrocatalytic activity, as evidenced by unaltered peak currents. However, the concurrent introduction of Fe_3O_4 under MF exposure induced a remarkable 2.1-fold enhancement in biocatalytic current density compared to the control SRB broth group. This synergistic effect demonstrates that the combination of MF and Fe_3O_4 is essential for augmenting the EET processes in *D. desulfuricans*.

The sulfate reduction results with X80 coupons as the sole electron donor further confirmed that MF enhances the EET behavior of *D. desulfuricans* (Fig. 8(b)). In cell-free medium, sulfate concentration showed no significant change, indicating that the coupons could not directly react with sulfate. However, in cell-inoculated medium, sulfate levels decreased significantly, as the cells utilized the metal (or hydrogen evolved from it) as an electron donor for sulfate reduction. Under MF conditions, the sulfate reduction was markedly higher than in the non-MF control, demonstrating that MF promotes EET in *D. desulfuricans*.

4. Discussion

4.1. Individual effects of the MF and SRB on the corrosion behavior

Experimental results indicate that MF can slightly accelerate abiotic corrosion processes. Our previous investigations have demonstrated that MF influence mass transfer processes through magnetohydrodynamic effects (Wang et al., 2022a). The magnetohydrodynamic forces primarily consist of paramagnetic gradient forces, Lorentz forces, and gradient magnetic forces (Wang et al., 2014). Under ambient temperature conditions, paramagnetic gradient forces are negligible (Weier et al., 2007). The gradient magnetic force, arising from electrochemical interactions of paramagnetic molecules in non-uniform MF, drives paramagnetic ions toward regions of higher magnetic flux density. In practical applications such as MFL testing for pipeline defects, localized flaws generate inherent non-uniform MF. Notably, Fahidy reported that the enhancement of limiting current (mass transfer current) by non-uniform MF is merely one-tenth of that achieved by uniform fields (Mohanta and Fahidy, 1978), thus justifying the negligible influence of gradient magnetic forces in our analysis.

Consequently, our investigation focuses primarily on the Lorentz force (F_L) governing mass transfer (Zhang et al., 2024c):

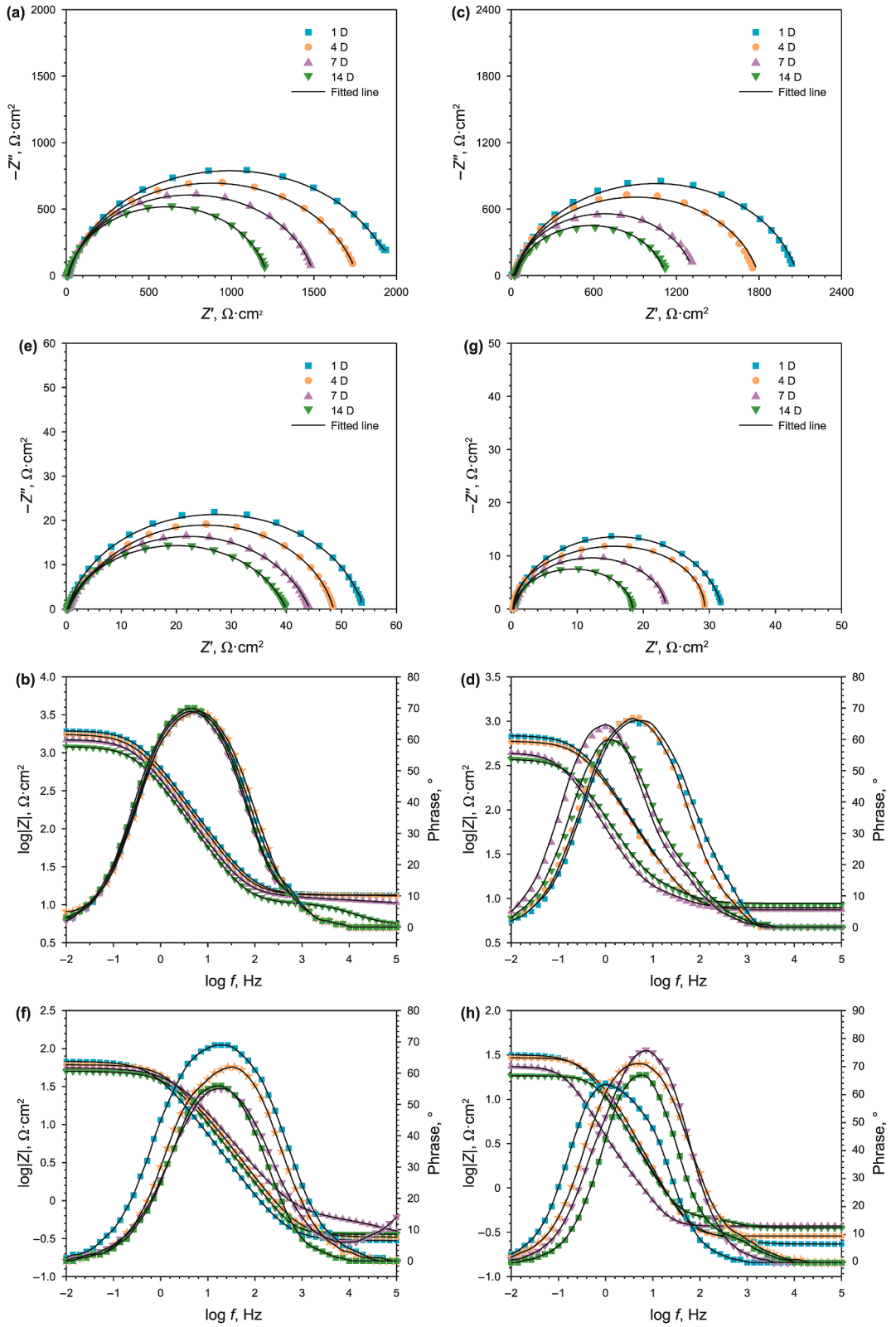

Fig. 7. Nyquist and Bode plot of X80 coupons: **(a)**–**(b)** control, **(c)**–**(d)** MF, **(e)**–**(f)** SRB, **(g)**–**(h)** MF + SRB.

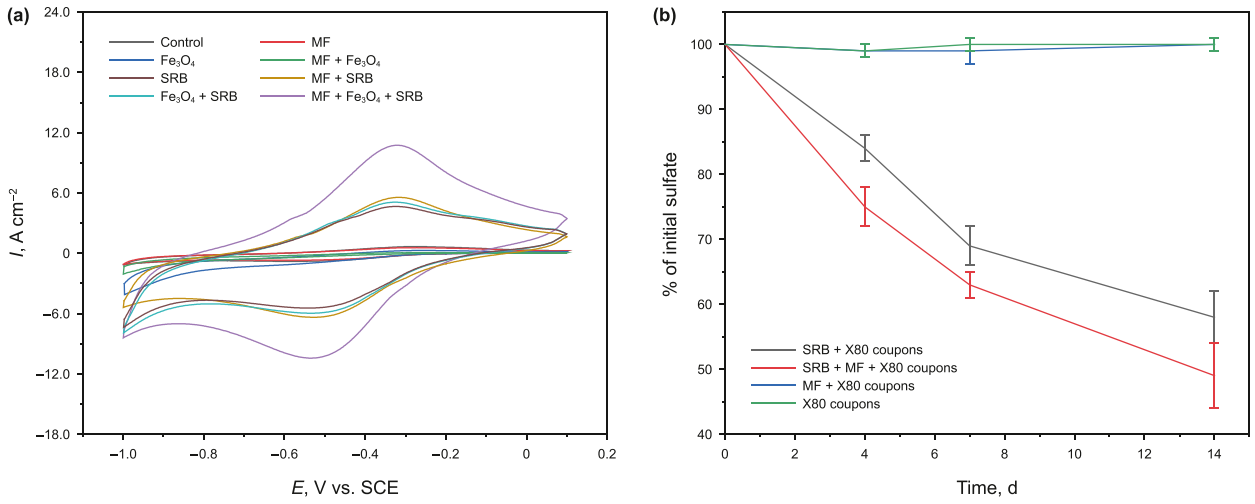

Fig. 8. **(a)** CV curves of X80 coupons after immersed in various conditions for 14 d, **(b)** sulfate reduction in the media after 14 d.

$$F_L = qv \times B \tag{1}$$

where q represents the electric charge of ions, v denotes ionic velocity, and B is the magnetic flux density.

The Lorentz force modifies ionic migration velocity through the relationship (Huang et al., 2019):

$$V_T = V_{mag} + V_{df} \tag{2}$$

where V_{df} corresponds to the velocity component induced by concentration gradients, and V_{mag} represents the Lorentz-induced velocity component. These findings collectively indicate that MF-enhanced mass transfer originates from magnetically induced convection. The intensified mass transfer reduces the thickness of the interfacial diffusion layer and modifies the concentration gradient of reactive species. During electrochemical processes exhibiting concentration polarization, this phenomenon manifests as a disparity between ion concentrations at the electrode surface and bulk solution. The resulting diffusion-limited current can be expressed as (Wang et al., 2022a):

$$I = \frac{nF}{V_l} D_i \frac{c_i^0 - c_i^s}{l} \tag{3}$$

where I is the steady diffusion current, l denotes the diffusion layer thickness, n the number of transferred electrons, F Faraday constant, V_l the flow rate, D_i the diffusion coefficient, and c_i^0 and c_i^s denote the surface concentration and the bulk phase concentration, respectively. The flow rate (V_l) induced by magnetic interactions directly influences the diffusion layer thickness, thereby modulating the overall mass transfer kinetics. However, in anaerobic environments, the cathodic reaction for corrosion is proton reduction rather than oxygen reduction. The diffusion rate of protons in solution is much higher than that of oxygen, so the effect of MF on abiotic corrosion is limited in anaerobic environments.

In SRB broth, cells exist in both planktonic and sessile forms. Planktonic cells are dispersed throughout the culture medium without direct contact with the coupon, whereas sessile cells adhere to the specimen surface and form biofilms. The typical metabolic reaction of SRB involves lactate as the organic electron donor to provide energy for cellular metabolism (Gu et al., 2019):

$$CH_3CHOHCOO^- + 2\,H_2O \rightarrow 2CH_3COO^- + CO_2 + 8H^+ + 8e^-$$

$$(E^{\circ\prime} = -430\ \text{mV}) \tag{4}$$

$$SO_4^{2-} + 9H^+ + 8e^- \rightarrow HS^- + 4H_2O\ (E^{\circ\prime} = -217\ \text{mV}) \tag{5}$$

However, within the biofilm, the dense EPS matrix impedes the diffusion of organic electron donors (e.g., lactate) to the underlying cell layers. Consequently, SRB cells in direct contact with the metal substrate cannot obtain sufficient metabolic energy from lactate. To sustain metabolism, these cells switch to extracting electrons directly from the metal (Wang et al., 2024c):

$$Fe \rightarrow Fe^{2+} + 2e^-\ (E^{\circ} = -447\ \text{mV}) \tag{6}$$

Since the oxidation potential of metallic iron (Fe^0) is lower than that of lactate, the coupling of iron oxidation with sulfate reduction yields a more negative Gibbs free energy (ΔG), making this pathway thermodynamically favorable. Thus, the utilization of Fe^0 as an alternative electron donor by SRB, facilitated by electron uptake from the metal surface, serves as a critical driving force for MIC. SRB cells uptake electrons from metallic iron (Fe^0) through several distinct mechanisms (Ueki and Lovley, 2022):1) direct electron uptake via outer membrane cytochrome proteins; 2) electron shuttle-mediated EET; 3) hydrogen (H_2) as an electron carrier derived from metal oxidation. In the medium with X80 steel as the sole electron donor, the SRB cells could consume sulfate, suggesting that *D. desulfuricans* caused MIC of X80 steel caused by EET (Fig. 8(b)).

4.2. Synergistic effect of the MF and SRB on the corrosion behavior

The corrosion test results showed that MF accelerated MIC. It has been demonstrated that Fe_3O_4 (magnetite) can compensate for deficiencies in outer membrane cytochromes and iron-oxidizing proteins (Liu et al., 2015; Jin et al., 2023), thereby enhancing EET. XPS analysis confirmed the presence of iron oxides (FeO, Fe_2O_3, and Fe_3O_4) in corrosion products. In MF condition, the sulfate consumption rate of *D. desulfuricans* was significantly higher than the environment without MF (Fig. 8(b)), indicating that MF accelerated the EET capability of *D. desulfuricans*. Notably, Fe_3O_4 possesses ferromagnetic properties, and the applied MF may have activated its role in promoting the EET of *D. desulfuricans*. Previous research results have shown

that the zeta potential of Fe_3O_4 is negative (Liu et al., 2022b), preventing its free adsorption onto steel surfaces, which hinders the ability of *D. desulfuricans* to utilize Fe_3O_4 for electron acquisition from metal surfaces. However, the applied MF could overcome this limitation through magnetic attraction, thereby facilitating EET. In addition, the MF stimulates the microbial dehydrogenase activity, which catalyzes the dehydrogenation of electron donors and transfers hydrogen atoms to electron acceptor (Łebkowska et al. 2018). In anaerobic environments, the abiotic cathodic reaction proceeds as:

$$H^+ + e^- \rightarrow H \ (E^\circ = 0 \text{ mV}) \quad (7)$$

Microbial dehydrogenases accelerate hydrogen ion reduction (cathodic reaction) while simultaneously promoting anodic metal dissolution (Eq. (6)). Furthermore, dehydrogenases transfer hydrogen atoms into microbial cells to supply electrons for sulfate reduction (Odom and Wall, 1987; Szczesny et al., 2020), preventing hydrogen accumulation—consistent with the classical cathodic depolarization theory. The bacterial cell, as a charged entity in MF, also generates Lorentz force, which reduces the ohmic losses during charge transfer between the cell and the electrode (Zhou et al., 2023; Liu et al., 2024). This improves the interfacial electron transfer efficiency. The MF accelerates MIC by promoting EET (Fig. 8(b)), thereby enhancing the ability of SRB to uptake electrons from the metal surface. This mechanistic distinction explains the observed differences in the effects of MF on abiotic corrosion and MIC (Fig. 9).

5. Conclusion

This study elucidates the influence mechanism of residual MF generated by magnetic flux leakage detection on MIC in subsea pipelines buried in sea mud. Our findings demonstrate that in a sterile environment, MF only slightly accelerate pipeline corrosion. However, MF exposure significantly exacerbates MIC induced by *D. desulfuricans*. Although the effect of MF on the growth and metabolic activity of *D. desulfuricans* is negligible, the MF stimulates EET by magnetite corrosion products (Fe_3O_4) deposited on the metal surface, thereby aggravating MIC. This investigation clearly reveals that residual MF produced by pipeline inspection gauge systems during magnetic flux leakage operations can accelerate MIC, highlighting the critical necessity of MF management to ensure the operational integrity of subsea pipelines. Pipeline steels should undergo demagnetization following MFL inspection to reduce residual magnetic effects. Furthermore, preventive strategies, including the use of biocides or antimicrobial coatings, are recommended to mitigate MIC.

CRediT authorship contribution statement

Ya-Jun Gai: Writing – original draft, Visualization, Validation, Investigation, Formal analysis, Data curation, Conceptualization. **Jia-Hang Li:** Writing – review & editing, Writing – original draft, Project administration, Formal analysis. **Fei Xie:** Writing – review & editing, Supervision, Resources, Project administration, Funding

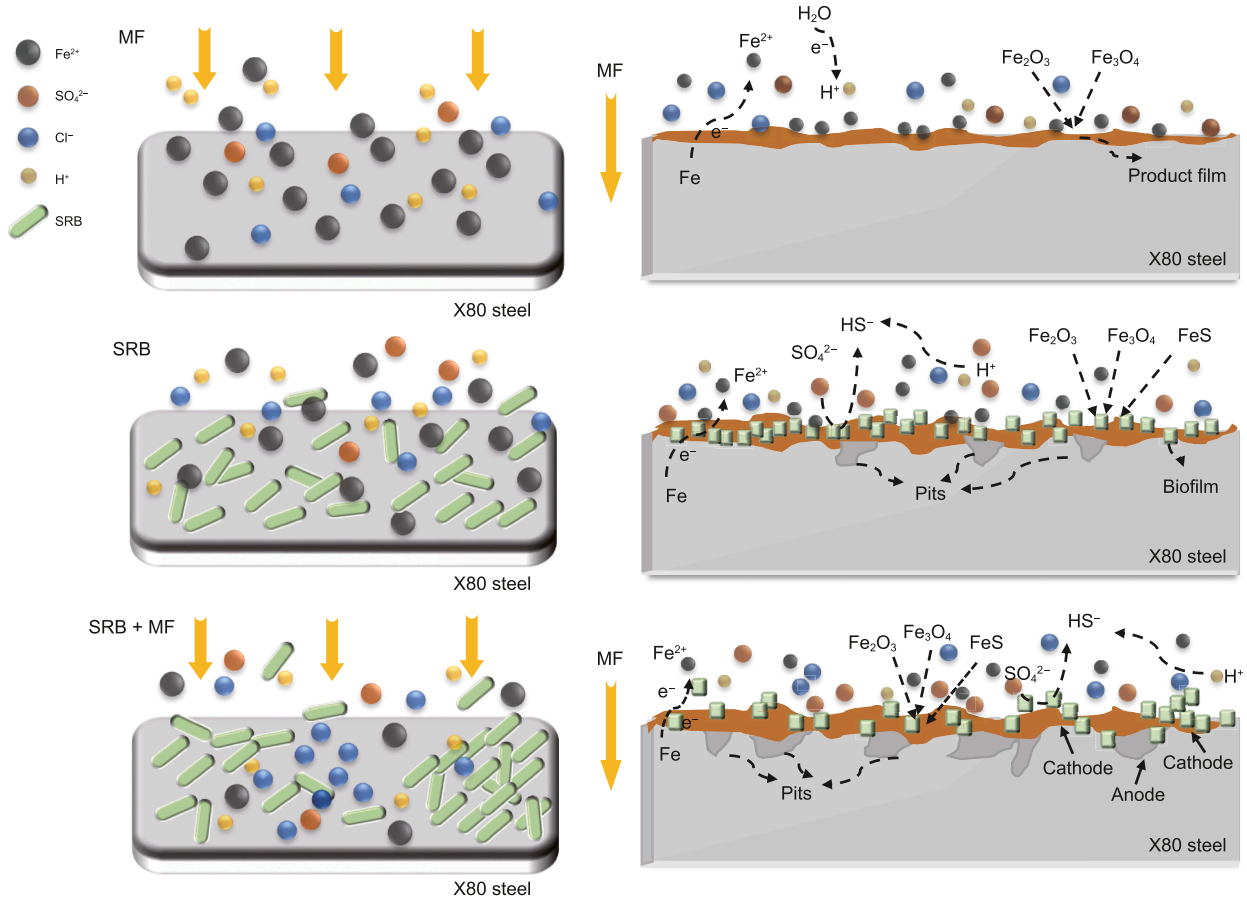

Fig. 9. Corrosion mechanism diagram of X80 steel under MF, SRB, and MF + SRB conditions.

acquisition, Data curation. **Dan Wang:** Project administration, Funding acquisition. **Dong-Xu Sun:** Project administration, Funding acquisition. **Yu-Xin Wang:** Visualization, Software, Formal analysis, Data curation. **Ming Wu:** Supervision, Project administration.

Declaration of competing interest

The authors declare that they have no known competing financial interests or personal relationships that could have appeared to influence the work reported in this paper.

Acknowledgments

This work was supported by the National Natural Science Foundation of China (Grant Nos. 52574085, 52402428, and 52404058).

Supplementary data

Supplementary data to this article can be found online at https://doi.org/10.1016/j.petsci.2026.01.023.

References

Alrammah, F., Xu, L.J., Patel, N., et al., 2024. Conductive magnetic nanowires accelerated electron transfer between C1020 carbon steel and *Desulfovibrio vulgaris* biofilm. Sci. Total Environ. 925, 171763. https://doi.org/10.1016/j.scitotenv.2024.171763.

Cristiani, P., Moradi, M., Basseguy, R., et al., 2025. Fundamentals and critical appraisal of electrochemical techniques for investigating microbial corrosion. Corros. Sci. 246, 112694. https://doi.org/10.1016/j.corsci.2025.112694.

Dinh, H.T., Kuever, J., Mußmann, M., et al., 2004. Iron corrosion by novel anaerobic microorganisms. Nature 427 (6977), 829–832. https://doi.org/10.1038/nature02321.

Gaines, R.H., 1910. Bacterial activity as a corrosion indeced in the soil. J. Ind. Eng. Chem. 2 (4), 128–130.

Gu, T.Y., Jia, R., Unsal, T., et al., 2019. Toward a better understanding of microbiologically influenced corrosion caused by sulfate reducing bacteria. J. Mater. Sci. Technol. 35 (4), 631–636. https://doi.org/10.1016/j.jmst.2018.10.026.

Hashemi, S.J., Bak, N., Khan, F., et al., 2017. Bibliometric analysis of microbiologically influenced corrosion (MIC) of oil and gas engineering systems. Corrosion 74 (4), 468–486. https://doi.org/10.5006/2620.

He, J.Y., Xie, F., Zhao, Y., et al., 2023. The effect of applied potential on stress corrosion cracking of X80 pipeline steel in acidic soil containing sulfate-reducing bacteria. Sci. China Technol. Sci. 66 (10), 2837–2849. https://doi.org/10.1007/s11431-022-2344-5.

Huang, M., Marinaro, G., Yang, X., et al., 2019. Mass transfer and electrolyte flow during electrodeposition on a conically shaped electrode under the influence of a magnetic field. J. Electroanal. Chem. 842, 203–213. https://doi.org/10.1016/j.jelechem.2019.04.043.

Javed, M.A., Ivanovich, N., Messinese, E., et al., 2024. The role of metallurgical features in the microbially influenced corrosion of carbon steel: a critical review. Microorganisms 12 (5), 892. https://doi.org/10.3390/microorganisms12050892.

Jia, R., Tan, J.L., Jin, P., et al., 2018. Effects of biogenic H_2S on the microbiologically influenced corrosion of C1018 carbon steel by sulfate reducing *Desulfovibrio vulgaris* biofilm. Corros. Sci. 130, 1–11. https://doi.org/10.1016/j.corsci.2017.10.023.

Jin, Y.T., Zhou, E.Z., Ueki, T., et al., 2023. Accelerated microbial corrosion by magnetite and electrically conductive pili through direct Fe^0-to-microbe electron transfer. Angew. Chem. Int. Ed. 62 (38), e202309005. https://doi.org/10.1002/anie.202309005.

Kuhr, C.A., Van, D.V., 1934. The graphitization of cast iron as an electrobiochemical process in anaerobic soils. Water 18, 147–165. https://doi.org/10.1140/epjp/s13360-022-02882-6.

Łebkowska, M., Rutkowska-Narożniak, A., Pajor, E., et al., 2018. Impact of a static magnetic field on biodegradation of wastewater compounds and bacteria recombination. Environ. Sci. Pollut. Res. 25 (23), 22571–22583. https://doi.org/10.1007/s11356-018-1943-0.

Lekbach, Y., Liu, T., Li, Y.C., et al., 2021. Microbial corrosion of metals: The corrosion microbiome. Adv. Micob. Physiol. 78, 317–390. https://doi.org/10.1016/bs.ampbs.2021.01.002.

Li, Z., Zhou, J.Y., Yuan, X.Y., et al., 2021. Marine biofilms with significant corrosion inhibition performance by secreting extracellular polymeric substances. ACS Appl. Mater. Interfaces 13 (39), 47272–47282. https://doi.org/10.1021/acsami.1c14746.

Li, J.R., Li, D.Y., Liang, D.B., et al., 2024. Static magnetic fields enhance microbial aggregation and adhesion to promote aerobic granulation. Chem. Eng. J. 489, 151392. https://doi.org/10.1016/j.cej.2024.151392.

Li, J.H., Zhou, E.Z., Xie, F., et al., 2025a. Accelerated stress corrosion cracking of X80 pipeline steel under the combined effects of sulfate-reducing bacteria and hydrostatic pressure. Corros. Sci. 243, 112593. https://doi.org/10.1016/j.corsci.2024.112593.

Li, J.H., Wang, D., Ouyang, X., et al., 2026. Bifunctional eco-friendly tobacco stem extract with antibacterial and corrosion inhibition properties for mitigating microbiologically influenced corrosion. J. Mater. Sci. Technol. 257, 46–59. https://doi.org/10.1016/j.jmst.2025.09.011.

Li, Y.Y., Wang, B.B., Wang, Y., et al., 2025b. Beneficial effect of heat input to improve microbial corrosion resistance of welded joint in X80 steel pipeline. J. Mater. Sci. Technol. 223, 217–234. https://doi.org/10.1016/j.jmst.2024.10.034.

Lin, Y., Chen, Y.T., Wang, H.Y., et al., 2024. Weak magnetic field promotes denitrification by stimulating ferromagnetic ion-containing metalloprotein expression. Water Res. 262, 122116. https://doi.org/10.1016/j.watres.2024.122116.

Liu, F.H., Rotaru, A.E., Shrestha, P.M., et al., 2015. Magnetite compensates for the lack of a pilin-associated c-type cytochrome in extracellular electron exchange. Environ. Microbiol. 17 (3), 648–655. https://doi.org/10.1111/1462-2920.12485.

Liu, H.W., Gu, T.Y., Zhang, G.A., et al., 2016. The effect of magneticfield on biomineralization and corrosion behavior of carbon steel induced by iron-oxidizing bacteria. Corros. Sci. 102, 93–102. https://doi.org/10.1016/j.corsci.2015.09.023.

Liu, H.W., Xu, D.K., Zheng, B.J., et al., 2018. A synergistic acceleration of corrosion of Q235 carbon steel between magnetization and extracellular polymeric substances. Acta Metall. Sin-Engl. 31 (5), 456–464. https://doi.org/10.1007/s40195-017-0666-4.

Liu, H.W., Chen, C.Y., Asif, M., et al., 2022a. Mechanistic investigations of corrosion and localized corrosion of X80 steel in seawater comprising sulfate-reducing bacteria under continuous carbon starvation. Corros. Commun. 8, 70–80. https://doi.org/10.1016/j.corcom.2022.08.002.

Liu, W.H., Pei, W.L., Moradi, M., et al., 2022b. Polyethyleneimine functionalized mesoporous magnetic nanoparticles with enhanced antibacterial and antibiofilm activity in an alternating magnetic field. ACS Appl. Mater. Interfaces 14 (16), 18794–18805. https://doi.org/10.1021/acsami.1c24148.

Liu, H.Z., Chen, T.Z., Li, J.C., 2024. Exogenous electric field as a biochemical driving factor for extracellular electron transfer: Increasing power output of microbial fuel cell. Energy Convers. Manag. 301, 118050. https://doi.org/10.1016/j.enconman.2023.118050.

Lu, S.H., Xue, N.T., Li, Z., et al., 2025. Influence of incubation time on corrosion behavior of EH36 steel by marine Halomonas titanicae in aerobic environments. J. Mater. Sci. Technol. 224, 257–266. https://doi.org/10.1016/j.jmst.2024.11.018.

Lu, S.H., Zhu, H.X., Xue, N.T., et al., 2024. Acceleration mechanism of riboflavin on Fe^0-to-microbe electron transfer in corrosion of EH36 steel by *Pseudomonas aeruginosa*. Sci. Total Environ. 939, 173613. https://doi.org/10.1016/j.scitotenv.2024.173613.

Ma, Q., Wang, Q., Zhou, X.B., et al., 2024. *Desulfovibrio desulfuricans* induced corrosion of welded joint in X80 pipeline steel below delaminated coating. Constr. Build. Mater. 411, 134335. https://doi.org/10.1016/j.conbuildmat.2023.134335.

Mohanta, S., Fahidy, T., 1978. Magnetoelectrolysis in non-uniform solenoidal fields. J. Appl. Electrochem. 8 (3), 265–267. https://doi.org/10.1007/BF00616429.

Odom, J., Wall, J., 1987. Properties of a hydrogen-inhibited mutant of *Desulfovibrio desulfuricans* ATCC 27774. J. Bacteriol. 169 (3), 1335–1337. https://doi.org/10.1128/jb.169.3.1335-1337.

Spruit, C., Wanklyn, J., 1951. Iron/sulphide ratios in corrosion by sulphate-reducing bacteria. Nature 168, 951–952. https://doi.org/10.1038/168951a0.

Sun, D.X., Wu, M., Xie, F., 2018. Effect of sulfate-reducing bacteria and cathodic potential on stress corrosion cracking of X70 steel in sea-mud simulated solution. Mat. Sci. Eng. A-Struct 721, 135–144. https://doi.org/10.1016/j.msea.2018.02.007.

Szczesny, J., Birrell, J., Conzuelo, F., et al., 2020. Redox-polymer-based high-current-density gas-diffusion H_2-oxidation bioanode using [FeFe] hydrogenase from *Desulfovibrio desulfuricans* in a membrane-free biofuel cell. Angew. Chem. Int. Ed. 59 (38), 16506–16510. https://doi.org/10.1002/anie.202006824.

Ueki, T., Lovley, D., 2022. *Desulfovibrio vulgaris* as a model microbe for the study of corrosion under sulfate-reducing conditions. mLife 1 (1), 13–20. https://doi.org/10.1002/mlf2.12018.

Wang, D., Li, T.J., Xie, F., et al., 2022a. Effect of magnetic field on the electrochemical corrosion behavior of X80 pipeline steel. Constr. Build. Mater. 350, 128897. https://doi.org/10.1016/j.conbuildmat.2022.128897.

Wang, D., Yang, C.t., Saleh, M.A., et al., 2022b. Conductive magnetite nanoparticles considerably accelerated carbon steel corrosion by electroactive *Desulfovibrio vulgaris* biofilm. Corros. Sci. 205, 110440. https://doi.org/10.1016/j.corsci.2022.110440.

Wang, L.Y., Li, J.H., Xie, F., et al., 2024a. Anions exacerbate microbial corrosion of X80 pipeline steel induced by sulfate-reducing bacteria in the sea mud environment. J. Electroanal. Chem. 973, 118705. https://doi.org/10.1016/j.jelechem.2024.118705.

Wang, X.H., Shi, Z.Z., Wang, Z.K., et al., 2024b. Electromagnetic field drives the bioelectrocatalysis of γ-Fe_2O_3-Coated Shewanella putrefaciens CN32 to boost extracellular electron transfer. Materials 17 (7), 1501. https://doi.org/10.3390/ma17071501.

Wang, Q., Wang, B.B., Zhou, X.B., et al., 2024c. Effects of carbon source starvation and riboflavin addition on selective corrosion of welded joint by *Desulfovibrio vulgaris*. Corros. Sci. 230, 111931. https://doi.org/10.1016/j.corsci.2024.111931.

Wang, X.P., Zhao, J.J., Hu, Y.P., et al., 2014. Effects of the Lorentz force and the gradient magnetic force on the anodic dissolution of nickel in HNO_3 + NaCl solution. Electrochim. Acta 117, 113–119. https://doi.org/10.1016/j.electacta.2013.11.100.

Wang, Y.X., He, J.Y., Xie, F., et al., 2023. The synergistic effect of parallel magnetic field and sulfate-reducing bacteria on stress corrosion cracking of buried X80 pipeline steel. Eng. Fail. Anal. 154, 107644. https://doi.org/10.1016/j.engfailanal.2023.107644.

Wanklyn, J.N., Spruit, C.J.P., 1952. Influence of sulphate-reducing bacteria on the corrosion potential of iron. Nature 169, 928–929. https://doi.org/10.1038/169928b0.

Weier, T., Eckert, K., Mühlenhoff, S., et al., 2007. Confinement of paramagnetic ions under magnetic field influence: Lorentz versus concentration gradient force based explanations. Electrochem. Commun. 9 (10), 2479–2483. https://doi.org/10.1016/j.elecom.2007.07.026.

Xu, D.K., Gu, T.Y., 2014. Carbon source starvation triggered more aggressive corrosion against carbon steel by the *Desulfovibrio vulgaris* biofilm. Int. Biodeterior. Biodegrad. 91, 74–81. https://doi.org/10.1016/j.ibiod.2014.03.014.

Zhang, T.S., Xu, Z.X., Wan, H.H., et al., 2024a. Dual corrosion promotion of pipeline steel in sea mud induced by sulfate reducing bacteria: bacteria concentration cell and electronic conduction of the biofilms covered sand grains. Corros. Sci. 232, 112005. https://doi.org/10.1016/j.corsci.2024.112005.

Zhang, Y.F., Zhou, E.Z., Wang, C.C., et al., 2024b. Microbiologically influenced corrosion of Ferrium M54 maraging steel with different grain sizes induced by *Desulfovibrio vulgaris*. Corros. Sci. 237, 112302. https://doi.org/10.1016/j.corsci.2024.112302.

Zhang, K.C., Wu, L.T., Wang, G.Y., et al., 2024c. Effects of magnetic fields on the formation of passive films on the surface of 5083 aluminum alloy. Corros. Sci. 235, 112163. https://doi.org/10.1016/j.corsci.2024.112163.

Zhao, S.L., You, Z.F., Zhang, X.W., et al., 2021. Magnetic field effects on the corrosion and electrochemical corrosion of Fe83Ga17 alloy. Mater. Char. 174, 110994. https://doi.org/10.1016/j.matchar.2021.110994.

Zheng, B.J., Li, K.J., Liu, H.F., et al., 2013. Effects of magnetic fields on microbiologically influenced corrosion of 304 stainless steel. Ind. Eng. Chem. Res. 53 (1), 48–54. https://doi.org/10.1021/ie402235j.

Zhou, H.H., Xuanyuan, X.W., Lv, X.W., et al., 2023. Mechanisms of magnetic sensing and regulating extracellular electron transfer of electroactive bacteria under magnetic fields. Sci. Total Environ. 895, 165104. https://doi.org/10.1016/j.scitotenv.2023.165104.